minerals

MDPI

Article

^{57}Fe Mössbauer Spectroscopy and X-ray Diffraction of Annealed Highly Metamict Perrierite: Activation Energy and Recrystallization Processes

Dariusz Malczewski [1,*], Agnieszka Grabias [2], Maria Dziurowicz [1] and Tomasz Krzykawski [1]

[1] Institute of Earth Sciences, University of Silesia, Będzińska 60, 41-200 Sosnowiec, Poland; maria.dziurowicz@us.edu.pl (M.D.); tomasz.krzykawski@us.edu.pl (T.K.)
[2] Łukasiewicz Research Network—Institute of Microelectronics and Photonics, Al. Lotników 32/46, 02-668 Warszawa, Poland; agnieszka.grabias@imif.lukasiewicz.gov.pl
* Correspondence: dariusz.malczewski@us.edu.pl

Abstract: This paper presents the results of ^{57}Fe Mössbauer spectroscopy and X-ray diffraction analysis of highly metamict perrierite $(REE,Ca,Th)_4(Fe^{2+},Mg)_2(Ti,Fe^{3+})_3Si_4O_{22}$ after annealing in argon from 673 to 1273 K for one hour. Radioactive elements in metamict minerals damage crystal structure on geologic time scales primarily due to recoil nuclei from α-decay of ^{238}U, ^{232}Th, ^{235}U, and their daughter products. Metamict minerals are widely used in geochronology and can serve as natural analogs for the study of radiation effects in high-level nuclear waste. Analyses were performed on fragments of a perrierite sample collected from granitoids near Amherst, Virginia (USA). Electron microprobe and gamma-ray spectrometry recorded Fe concentrations of 4.7 wt.% and Th and U concentrations of 0.64 and 0.06 wt.%, respectively. The calculated total absorbed α-dose was 7.8×10^{15} α-decay mg^{-1}. The Mössbauer spectrum of the untreated sample can be fitted to two Fe^{2+} and two Fe^{3+} doublets in octahedral coordination with a relative $\Sigma Fe^{2+}/\Sigma Fe$ of 0.63. For samples annealed at 1173 K and 1273 K, spectra show a decrease in the total contribution of Fe^{2+} to 0.58 due to dehydroxylation associated with the simultaneous oxidation of post-metamict Fe^{2+} to Fe^{3+}. In the examined perrierite, Fe^{2+} occurs in structural positions B and C(1). The broad, predominant Fe^{3+} doublet observed in the spectrum of the unannealed sample splits into two components at 973 K interpreted to represented positions C(1) and C(2) in the perrierite structure. The Mössbauer spectra show a prominent decrease in the width of the high-energy absorption peak representing Fe^{2+} components with increasing temperature. The variation in the width of this peak versus the annealing temperature seems to be an indicator of thermally induced recrystallization. Based on the exponential dependence of the derivative function of the parameter with the inverse temperature and using an Arrhenius plot, an activation energy (E_A) of 0.73 eV was determined for thermally-induced recrystallization. Corresponding XRD data show progressive recrystallization with increasing annealing temperature. The XRD pattern of the fragment annealed at 1273 K indicates that highly metamict perrierite recrystallized to the pre-metamict state that can be indexed to the C2/m space group.

Keywords: metamict perrierite; Mössbauer spectroscopy; X-ray diffraction; high-temperature annealing; activation energy

Citation: Malczewski, D.; Grabias, A.; Dziurowicz, M.; Krzykawski, T. ^{57}Fe Mössbauer Spectroscopy and X-ray Diffraction of Annealed Highly Metamict Perrierite: Activation Energy and Recrystallization Processes. *Minerals* **2023**, *13*, 1395. https://doi.org/10.3390/min13111395

Academic Editor: Michael Oshtrakh

Received: 11 September 2023
Revised: 27 October 2023
Accepted: 28 October 2023
Published: 30 October 2023

1. Introduction

Perrierite is a REE-Ti-bearing accessory mineral often found in a metamict state due to the presence of Th and, to a lesser degree, U in its crystal structure. It was first recorded in shore sands of Nettuno, Italy in 1950 [1]. Perrierite shows a strong chemical and structural similarity to chevkinite, and previous works have suggested that it is the same mineral [2]. Later studies reported that these are distinct minerals with slight structural differences [3–7]. The perrierite-chevkinite mineral group (sorosilicates) can be represented by the idealized formula $A^{3+}{}_4B^{2+}C^{3+}{}_2Ti^{4+}{}_2Si_4O_{22}$, where A = REE, Th, Ca, Sr, Na, and K in 8- and 10-fold

coordination, B = Fe^{2+}, Mg, Mn, and Ca in 6-fold coordination, and C = Ti, Mg, Mn, Fe^{3+}, Fe^{2+}, Nb, Al, and Zr in 6-fold coordination. Cerium (Ce) represents the dominant rare earth element, and many substitutions are possible [8–11].

The proposed polyhedral representation of chevkinite–perrierite group minerals [11] consists of four octahedrally coordinated M-sites, where the M(1) site is predominantly occupied by Fe^{2+} (position B), and the remaining M(2), M(3), and M(4) sites are occupied primarily by Ti and Fe^{3+} (positions C(2) and C(1)) [8]. Position A consists of two polyhedra, A(1) and A(2), with respective coordination numbers of 8 and 10. The remarkable similarity of both minerals raises the possibility that they may be polymorphs. Studies on synthetic chevkinites and perrierites have shown that the size of the cations at the A, B, and C positions determines which phase will be formed, and they do not qualify as polymorphs according to the formal definition [6]. Substitutions of a wide range of cations make natural minerals more complicated, however, and the crystal structure in question generally exhibits behaviors similar to synthetic equivalents. Chevkinite–perrierite group minerals exhibit polymorphism or polymorphic behavior during temperature-induced transitions. The report [4] describes how three out of five samples of chevkinite annealed under atmospheric air at temperatures of 1000 °C and 1350 °C transformed into perrierite within one hour. The transformations did not occur among samples annealed in argon, nor was the reverse transition (perrierite to chevkinite) observed during annealing under atmospheric air at the same temperatures. These observations have led to the suggestion that perrierite is oxidized chevkinite. This result was partially confirmed for a sample of chevkinite from Virginia [5]. Extensive studies of synthetic chevkinites and perrierites have shown the opposite behavior. Compounds crystallized as perrierites transition to the chevkinite after heating at 1070 °C [7]. In general, among natural and synthetic minerals, thermal polymorphism can be observed for specimens or compounds whose chemical composition lies close to a phase boundary. These may transform from one phase to another due to a small change in the ratio of ionic sizes.

This study used Mössbauer spectroscopy and X-ray diffraction to trace the recrystallization process of highly metamict perrierite following high-temperature annealing in argon. To our knowledge, no published literature has addressed transformation of local crystal structure around Fe ions during annealing of metamict perrierite. Mössbauer spectroscopy results were also used to determine the activation energy for thermally induced recrystallization of highly metamict perrierite. The activation energy helps determine the sensitivity of metamict phases to amorphization and thermal recrystallization. The higher the activation energy for thermal recrystallization, the easier it will be for a mineral to become amorphized by radiation damage due to recoil nuclei from α-decay of U and Th series constituents. Table 1 summarizes the limited data available on activation energies (obtained by different methods) for recrystallization processes in metamict minerals.

Table 1. Previously reported activation energies for metamict minerals.

Reference	Mineral	Activation Energy (eV)	Methods
[12]	Allanite	2.3	Fission track annealing
[13]	Microlite (partially metamict)	0.33	DTA
	Betafite (metamict)	0.97	
[14]	Zircon	2.87	Fission track annealing
		3.59	Heavy ion track annealing
[15]	Gadolinite (partially metamict)	0.58	X-ray diffraction
[16]	Monazite	0.08	Irradiation by 800 keV Kr^{2+}
[17]	Gadolinite (metamict)	1.97	Mössbauer spectroscopy
[18]	Davidite (partially metamict)	0.45	Mössbauer spectroscopy

2. Materials and Methods

2.1. Sample Description and Chemical Analysis

The perrierite–(Ce) example investigated here exhibits mostly grayish black and vitreous luster with some dull areas (Figure 1). It was collected from a pegmatite near Amherst, Virginia (USA) [5]. After splitting the large sample into fragments, the pieces were placed in quartz tubes, sealed under argon, and annealed for one hour in a muffle furnace at 673, 773, 973, 1073, 1173, and 1273 K. Each temperature was stabilized within ±2 K. After annealing, the samples were quenched and ground to a powder.

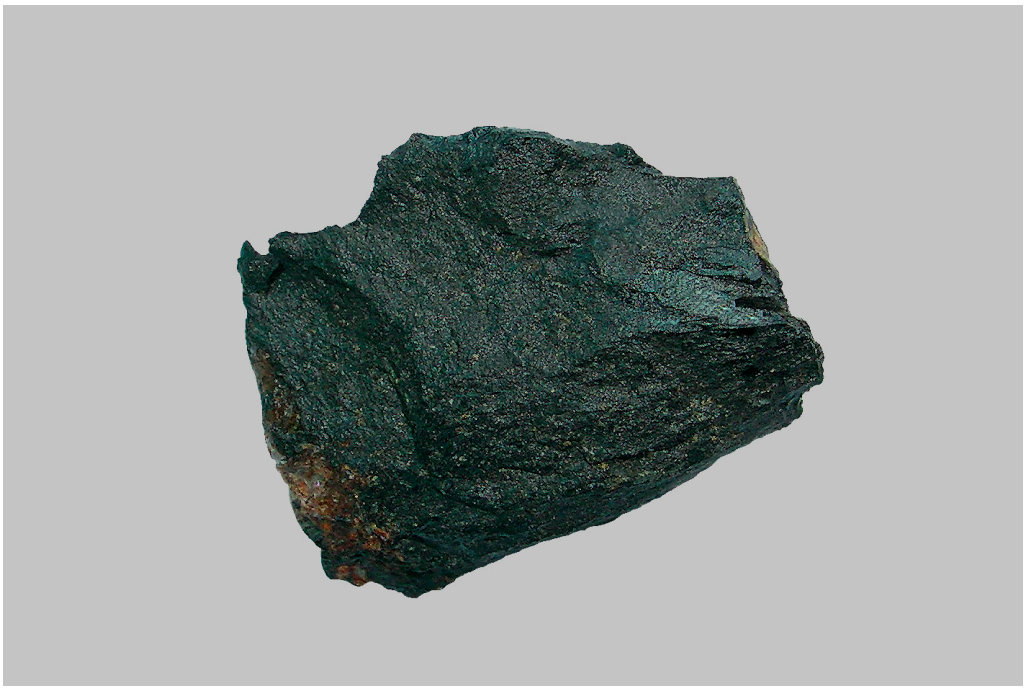

Figure 1. Photo of one of the perrierite specimens from Amherst (Virginia) analyzed in this study. The long edge is 2.5 cm in length.

The composition of the sample was determined using a JEOL JSM-6480 scanning electron microscope with an energy-dispersive X-ray spectrometer (SEM–EDS) operated at an accelerating voltage of 20 kV and a beam current of 30 μA. Data were analyzed using the EDS2006 software package. Electron-microprobe data were obtained from two inner fragments of the specimen subjected to 26 total analytical points. The concentrations of ^{232}Th, ^{238}U, and ^{235}U were calculated based on gamma-ray activities of ^{228}Ac (^{232}Th), ^{226}Ra, ^{214}Pb, and ^{214}Bi (^{238}U), and assuming a natural ^{238}U/^{235}U ratio of 137.88 [19]. Gamma-ray spectra were collected using a GX4018 system consisting of a coaxial HPGe detector (45.2% efficiency) in a lead and cooper shield (102 mm) with a Lynx multichannel buffer. Table 2 lists the chemical composition and the calculated α-doses.

The studied perrierite exhibited a total absorbed α-dose of 7.8×10^{15} α-decay mg^{-1} (Table 2). The calculated ^{232}Th α-dose of 5.5×10^{15} α-decay mg^{-1} was more than twice that of ^{238}U (2.1×10^{15} α-decay mg^{-1}). The sample also exhibited high Nd content (6.2 wt.%). Similar Nd concentrations were noted for samples from two localities near Amherst in one of the first published reports on perrierites and chevkinites from Virginia [5].

Table 2. Age, chemical composition (wt.%), and calculated α-doses for the perrierite sample examined in this study.

Age	1.1(1) Ga [a]
O	26.3(14)
F	1.08(43)
Al	2.7(10)
Si	13.9(9)
Ca	4.6(18)
Ti	8.3(17)
Fe	4.7(10)
Ge	0.72(20)
Se	1.49(24)
Rb	1.81(10)
Zr	0.42(24)
Nb	0.54(26)
Ce	15.9(17)
Nd	6.2(10)
La, Gd, Er, Yb, Lu	7.9(12)
Ta	1.97(41)
Th	0.64(3)
U	0.060(3)
Total	99.23
Calculated total dose (D_T) [b] (α-decay mg^{-1})	$7.77(78) \times 10^{15}$
Calculated dose from ^{232}Th (D_{232}) (α-decay mg^{-1})	$5.54(53) \times 10^{15}$
Calculated dose from ^{238}U (D_{238}) (α-decay mg^{-1})	$2.09(23) \times 10^{15}$
Calculated dose from ^{235}U (D_{235}) (α-decay mg^{-1})	$0.14(2) \times 10^{14}$

[a] Mesoproterozoic age. [b] Doses were calculated as: $D_{232} = 6 \times N_{232}(e^{t\,\lambda 232} - 1)$, $D_{238} = 8 \times N_{238}(e^{t\,\lambda 238} - 1)$, $D_{235} = 7 \times N_{235}(e^{t\,\lambda 235} - 1)$, and $D_T = D_{232} + D_{238} + D_{235}$. N_{232}, N_{238}, and N_{235} are the present number of atoms of ^{232}Th, ^{238}U, and ^{235}U per milligram, λ_{238}, λ_{235}, and λ_{232} are the decay constants of ^{232}Th, ^{238}U, and ^{235}U (respectively), and t is the geologic age.

2.2. Mössbauer Spectroscopy and X-ray Diffraction

For ^{57}Fe Mössbauer spectroscopy, the powder fragments were prepared as a thin disc absorber with surface densities close to 10 mg cm^{-2}. Mössbauer transmission spectra of the untreated and annealed fragments were recorded at room temperature using a constant acceleration spectrometer with a linear velocity reference signal of triangular shape in the range of ±4.5 mm s^{-1}, and a linear arrangement of a $^{57}Co/Rh$ source (=50 mCi, 295 K), an absorber, and a proportional counter. For each sample, a few million counts per channel were collected by a multichannel analyzer in 512 channels and then folded to 256 channels. Mössbauer spectra were numerically analyzed by the fitting software Recoil, and all doublets were fitted with Lorentz lines. The velocity scale was calibrated using α-Fe foil about 25 μm thick as a reference absorber at 295 K, and the calibration spectrum was fitted using Lorentz lines with the full width at a half maximum of 0.27 mm s^{-1}.

The untreated and annealed fragments were analyzed for their X-ray diffraction (XRD) patterns using a PANanalytical X'Pert PRO MPD diffractometer in the Θ−Θ system and CoKα radiation in the scan mode with a 0.02° step size and a 298 s counting time for each step. Computational analyses were performed using HIGHSCORE+ PANanalytical v.4.6 software. Numerical calculations to determine the activation energy were performed using the OriginPro 2023b software (OriginLab Corporation, Northampton, MA, USA).

3. Results and Discussion

3.1. Mössbauer Spectroscopy

Figures 2 and 3 show ^{57}Fe Mössbauer spectra and the corresponding XRD patterns of the respective untreated and annealed perrierite samples as a function of annealing temperature. Table 3 lists the hyperfine parameters derived from the fitting procedure for each annealed sample. Isomer shift values are given relative to the α-Fe standard.

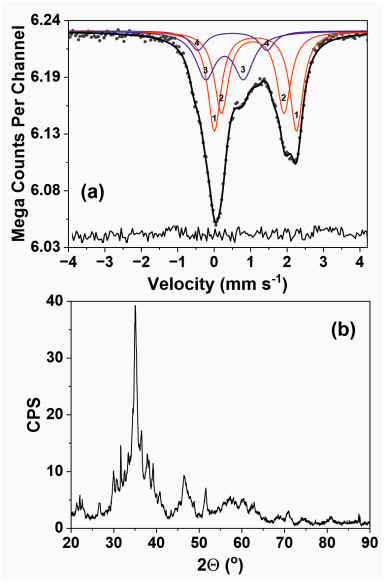

Figure 2. (**a**) ^{57}Fe Mössbauer spectrum of untreated perrierite sample. Solid dots = experimental data, thick solid line = fitted curve, thin solid line = fitted doublets; (**b**) corresponding XRD pattern.

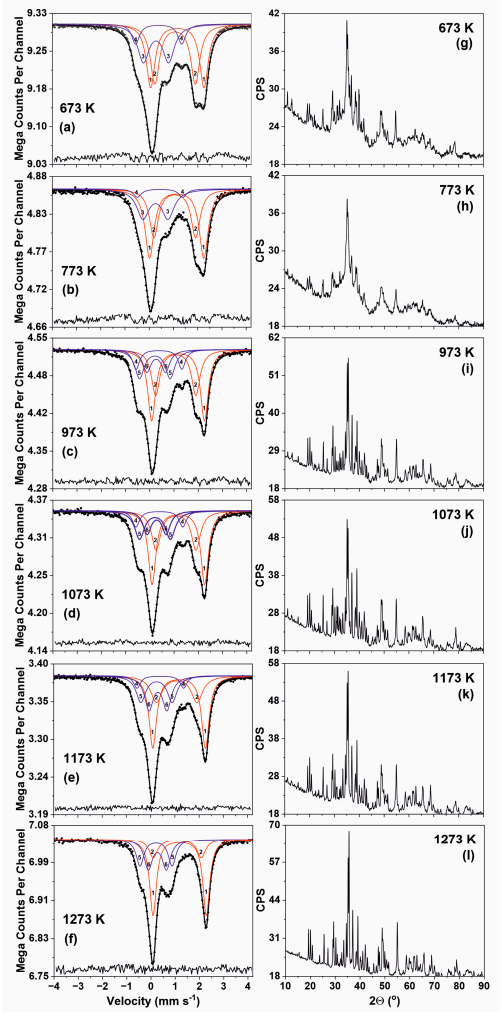

Figure 3. (**a**–**f**) ^{57}Fe Mössbauer spectra at room temperature of perrierite samples annealed in argon for 1 h at the given annealing temperatures. Solid dots = experimental data, thick solid line = fitted curve, thin solid line = fitted doublets; (**g**–**l**) corresponding XRD patterns.

Table 3. Parameters for ^{57}Fe Mössbauer spectra for untreated sample (UT) and annealed perrierite samples (Figure 3).

Annealing Temperature (K)	Doublet No.	χ^2	δ (mm s^{-1})	Δ (mm s^{-1})	Γ (mm s^{-1})	Assignment (CN)	Rel. Area *
UT							
	1	1.61	1.13(1)	2.25(2)	0.44(1)	Fe^{2+}(6)	0.37
	2		1.07(1)	1.73(2)	0.44(2)	Fe^{2+}(6)	0.30
	3		0.32(2)	1.02(5)	0.70(3)	Fe^{3+}(6)	0.26
	4		0.49(4)	1.99(4)	0.50(3)	Fe^{3+}(6)	0.07
673							
	1	0.97	1.15(1)	2.20(1)	0.42(1)	Fe^{2+}(6)	0.33
	2		1.06(1)	1.67(2)	0.44(1)	Fe^{2+}(6)	0.32
	3		0.28(2)	1.04(1)	0.58(1)	Fe^{3+}(6)	0.25
	4		0.39(1)	1.90(2)	0.38(2)	Fe^{3+}(6)	0.10
773							
	1	1.80	1.13(1)	2.23(2)	0.44(1)	Fe^{2+}(6)	0.42
	2		1.05(1)	1.72(1)	0.44(1)	Fe^{2+}(6)	0.25
	3		0.26(1)	1.03(3)	0.62(2)	Fe^{3+}(6)	0.27
	4		0.44(3)	1.87(4)	0.40(3)	Fe^{3+}(6)	0.06
973							
	1	1.34	1.17(1)	2.18(1)	0.38(1)	Fe^{2+}(6)	0.36
	2		1.07(1)	1.66(1)	0.42(1)	Fe^{2+}(6)	0.25
	4		0.38(1)	1.89(1)	0.36(1)	Fe^{3+}(6)	0.10
	5		0.21(1)	1.26(3)	0.46(3)	Fe^{3+}(6)	0.17
	6		0.27(1)	0.77(4)	0.42(1)	Fe^{3+}(6)	0.12
1073							
	1	1.15	1.18(1)	2.17(1)	0.38(1)	Fe^{2+}(6)	0.38
	2		1.08(1)	1.64(2)	0.44(2)	Fe^{2+}(6)	0.24
	4		0.39(1)	1.93(1)	0.36(3)	Fe^{3+}(6)	0.08
	5		0.21(1)	1.27(1)	0.48(3)	Fe^{3+}(6)	0.18
	6		0.28(1)	0.78(1)	0.40(1)	Fe^{3+}(6)	0.12
1173							
	1	0.95	1.18(1)	2.17(1)	0.38(1)	Fe^{2+}(6)	0.37
	2		1.08(1)	1.67(2)	0.56(3)	Fe^{2+}(6)	0.20
	4		0.40(2)	1.92(3)	0.34(2)	Fe^{3+}(6)	0.06
	5		0.24(1)	1.29(1)	0.48(3)	Fe^{3+}(6)	0.17
	6		0.30(1)	0.74(2)	0.44(2)	Fe^{3+}(6)	0.20
1273							
	1	1.54	1.19(1)	2.19(1)	0.32(1)	Fe^{2+}(6)	0.38
	2		1.08(1)	2.02(2)	0.56(3)	Fe^{2+}(6)	0.20
	5		0.23(1)	1.34(3)	0.44(2)	Fe^{3+}(6)	0.19
	6		0.29(1)	0.72(3)	0.44(2)	Fe^{3+}(6)	0.23

* Estimated uncertainty is $\Delta A/A \leq 10\%$.

The Mössbauer spectrum of the untreated sample shows two quadrupole doublets assigned to Fe^{2+} (nos. 1 and 2) and two quadrupole doublets assigned to Fe^{3+} (nos. 3 and 4), all in octahedral coordination (Figure 2a, Table 3). The powder XRD pattern (Figure 2b) shows that the untreated sample is highly metamict with an absorbed α-dose of 7.8×10^{15} α-decay mg^{-1}. Previous studies suggest that the amorphization dose approaches 10^{16} α-decay mg^{-1} for metamict silicates and 10^{17} α-decay mg^{-1} for metamict oxides [20–25].

3.1.1. Changes in Fe^{2+} Components

For the unannealed sample, doublet no. 1 with δ = 1.13 mm s^{-1} and Δ = 2.25 mm s^{-1} makes the largest contribution (0.39 on average) to Mössbauer spectra across all annealing temperatures. This doublet's δ and Δ values are almost the same for samples annealed from 673 K to 1273 K and average 1.17 mm s^{-1} and 2.19 mm s^{-1}, respectively. These values indicate the relatively regular coordinating octahedra. According to the accepted

description of the structure of the chevkinite–perrierite group, this doublet should be assigned to Fe^{2+} in position B and to the M1 site in the polyhedral representation.

Relative to doublet no. 1, doublet no. 2 consists of a Fe^{2+} component with noticeably smaller values representing an isomer shift and a quadrupole splitting. The unannealed sample and samples annealed from 673 K to 1173 K yielded average δ and Δ values of 1.07 mm s^{-1} and 1.68 mm s^{-1}, respectively. This contribution decreased with increasing annealing temperature and a simultaneous increase in doublet no. 6 from Fe^{3+} (Figure 3, Table 3). The Fe^{2+} doublets with low δ and Δ values mostly appeared in octahedral positions showing tetragonal deformation, including radiation-damaged metamict minerals [26–29]. After recrystallization at 1273 K, this doublet exhibited higher quadrupole splitting (2.02 mm s^{-1}) values, while the isomer shift did not change (Table 3). Hyperfine parameters for doublet no. 2 and the observed increase in the doublet no. 6 contribution from Fe^{3+} indicate that this component represents Fe^{2+} at the C(1)/M2 position. The perrierite structure shows that both Fe^{2+} and Fe^{3+} are present in this position. As seen in Figure 4, the relative contribution of ΣFe^{2+} varies from 0.56 to 0.67. The observed decrease in the contribution of Fe^{2+} above 773 K most likely reflects Fe^{3+} reduction to Fe^{2+} in damaged mineral regions due to post-damage diffusion of H_2 (as OH^-) into the structure. Conversely, recrystallization in argon can be accompanied by dehydroxylation with simultaneous oxidation of excess post-metamict Fe^{2+} to Fe^{3+}. This effect was observed in davidite and titanite [18,30]. The large contribution of doublet no. 2 in spectra for the unannealed sample and those annealed at lower temperatures results from the metamictization process. In untreated allanite–(Ce) specimens with various degrees of metamictization, the ratio of ΣFe^{2+} to ΣFe varied from 0.40 to 0.73 [31,32]. For a sample of fully metamict allanite, heating in atmospheric air at 1000 K causes only partial oxidation of Fe^{2+} to Fe^{3+} [32]. The metamict state strengthens the Fe^{2+} fraction.

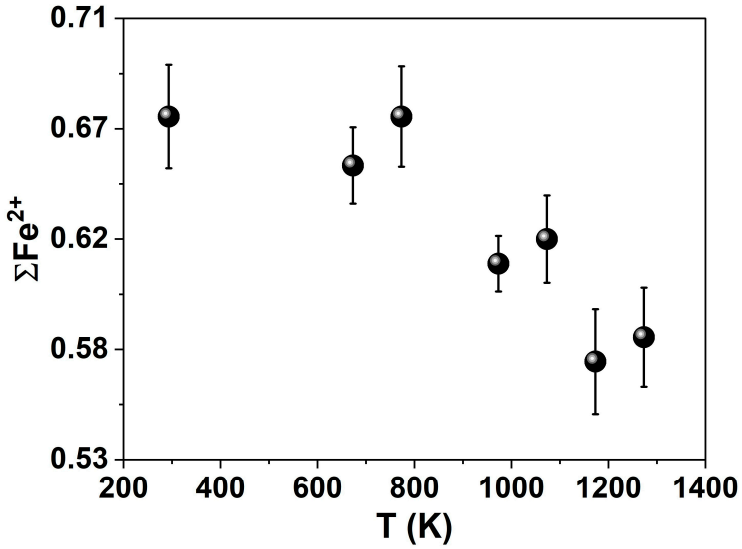

Figure 4. Relative contributions of Fe^{2+} vs. annealing temperature.

According to the perrierite structure, the bond lengths of Fe with apex oxygens, e.g., Fe−O(7) or Fe–O(6) [8,11], should be significantly shorter, by about 0.15–0.20 Å, relative to the average bond length of the other four coordinating oxygens in the M1 site. In the Mössbauer spectrum, the component derived from such a Fe^{2+} position should be characterized by hyperfine parameters similar to those observed for doublet no. 2 up to 1173 K. However, according to the δ and Δ values, doublet no. 1 represents a more regular octahedral site.

The only known published report of the Mössbauer spectrum of a chevkinite sample shows two Fe^{2+} doublets with a total contribution of 0.43 [33]. The first with a contribution

of 0.09 and δ and Δ values of 1.25 mm s^{-1} and 2.21 mm s^{-1}, respectively, was assigned to Fe^{2+} in the eight-coordinated A site. A feature with these parameters did not appear in our data. The second doublet assigned to position B, representing a contribution of 0.34 (within error), and with values of δ = 1.14 mm s^{-1} and Δ = 2.25 mm s^{-1}, corresponds exactly to doublet no. 1 in the perrierite spectra. The authors did not describe the degree of metamictization of the chevkinite sample, but fitted line widths suggest that the sample was partially metamict.

3.1.2. Changes in Fe^{3+} Components

As previously noted, in the spectrum of the unannealed perrierite sample, Fe^{3+} iron is represented by two doublets numbered 3 and 4. The large width of doublet no. 3 absorption line indicates that it results from a larger number of slightly different but overlapping Fe^{3+} components with a continuous δ and Δ distribution. This would result from the deformation of the coordinating octahedrons during metamictization. Starting at 973 K, doublet no. 3 was divided into two new components labeled as doublets 5 and 6 (Figure 3c–f, Table 3). Doublet no. 5 for samples annealed from 973 K to 1273 K exhibits a low isomer shift averaging 0.22 mm s^{-1} and a relatively high quadrupole splitting averaging 1.29 mm s^{-1}. The contribution of this doublet changed slightly from 0.17 to 0.19. The isomer shift and quadrupole splitting values indicate that this doublet represents the C(2)/M4 position in the perrierite structure. Based on studies of synthetic perrierite crystals [8], position C(2) may have extremely different bond lengths of 1.79 Å and 2.42 Å for the two coordinating oxygens. This causes a very strong interaction with the former and a weak interaction with the latter. Such asymmetric octahedra can yield the Fe^{3+} component with hyperfine parameters observed for doublet no. 5.

Doublet no. 6 is characterized by an average δ of 0.29 mm s^{-1} and an average Δ of 0.75 mm s^{-1}, as well as an increasing contribution from 0.12 to 0.23 in the spectrum of the sample annealed at 1273 K (Figure 3f, Table 3). The increase in the contribution of this doublet reflects the decrease in the doublet no. 2 Fe^{2+} contribution. These observations, along with the hyperfine parameter values, suggest a doublet assignment to the C(1)/M2 position [8–11]. The average value of isomer shifts and quadrupole splittings of doublets 5 and 6 indicate octahedral coordination of Fe^{3+}. The Fe^{3+} in tetrahedral coordination should be characterized by δ ~ 0.17 mm s^{-1} and Δ~ 0.50 mm s^{-1}, respectively. Such components do not occur in the examined perrierite [34,35].

Doublet no. 4 present in the Mössbauer spectra of samples annealed at 1173 K exhibits the highest average δ value of 0.42 mm s^{-1}, Δ equal to 1.92 mm s^{-1} and also the smallest contribution of previously discussed Fe^{3+} components (Figure 3, Table 3). As indicated by its absence in the fully crystalline sample after annealing at 1273 K and the slight increase in doublet 5 and 6 contributions, this doublet probably represents the most distorted Fe^{3+} octahedra at the M2 and M4 sites.

In chevkinite, two Fe^{3+} doublets were reported with hyperfine parameter values of δ = 0.43 mm s^{-1} and Δ = 0.57 mm s^{-1}, and δ = 0.33 mm s^{-1} and Δ = 1.34 mm s^{-1}, respectively, with contributions of 0.36 and 0.21, respectively. These correspond to doublets 6 and 5 in the spectra of the studied perrierite. The data indicate lower isomer shifts by the main perrierite Fe^{3+} components relative to their structural counterparts in the chevkinite analyzed thus far. The relations also suggest potentially smaller-sized Fe^{3+} octahedra in perrierite relative to those in chevkinite [33].

3.2. Unit Cell Parameters

Figure 3g–l shows XRD diffraction patterns for perrierite samples after one hour of annealing in argon at 673, 773, 973, 1073, 1173, and 1273 K. The data show samples recrystallizing with increasing temperature and complete crystallization with sample annealing at 1273 K.

Table 4 lists the cell parameters for the best fit obtained for the C2/m space group after XRD data processing. Figure 5 shows the high degree of agreement between experimental XRD patterns and those calculated for the C2/m space group.

Table 4. Unit cell dimensions calculated for metamict perrierite after one-hour annealing at 1273 K in argon.

Name	Value
Unit Cell	C 1 2/m 1
a (Å)	13.5841(8)
b (Å)	5.6340(3)
c (Å)	11.6722(3)
alpha (°)	90
beta (°)	113.38(2)
gamma (°)	90
V (Å^3)	818.3592

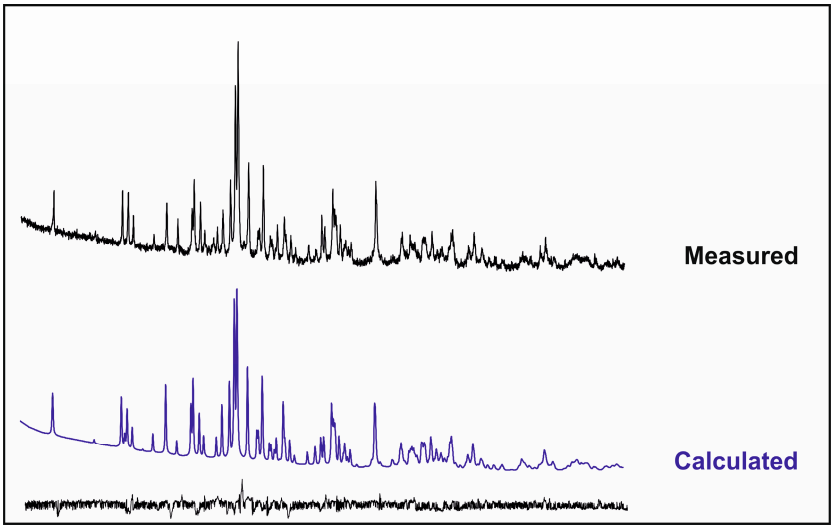

Figure 5. Comparison of XRD pattern for a perrierite sample annealed in argon at 1273 K for one hour (top) and a calculated XRD pattern for the C2/m space group (bottom).

The unit cell parameters of the annealed perrierite sample match those reported for natural and synthetic perrierites. The main lattice parameter that distinguishes perrierite from chevkinite is the "β" lattice constant, which ranges from 113.4° to 113.9° for perrierite and from 100.2° to 101° for chevkinite. In the case of the perrierite sample annealed in this study, the parameter's value is 113.6°.

3.3. Determination of Activation Energy

The metamictization process causes deformation and displacement of structural polyhedra. Thermal recrystallization restores the structural units to position, obtaining crystalline forms. The activation energy for thermally induced recrystallization of a metamict mineral represents the minimum energy required to restore structural polyhedra and, consequently, the original long-range order that defines the crystalline state. As seen in Figure 3a–f, the absorption line width of the high energy peak from Fe^{2+} components (nos. 1 and 2) decreases with increasing annealing temperature. This allows a parameter R (Figure 6a,b) to be defined so as to represent the ratio of the line width of the untreated sample (Γ_{UT}) to the line width of samples annealed at temperature T (Γ_T). The R term can then serve as input data for estimating the activation energy for recrystallization from Mössbauer spectroscopy data based on existing annealing models [14,36,37].

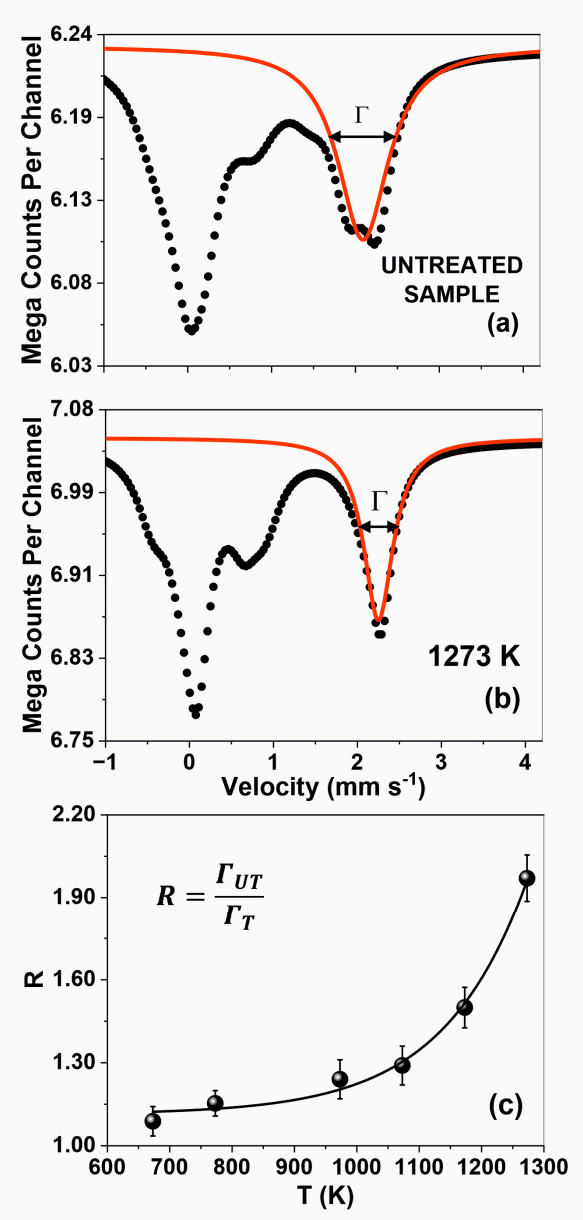

Figure 6. (**a**,**b**) represent the width at half maximum of the high-energy peak (Γ) from Fe^{2+} components fitted with the Lorentzian singlet; (**c**) variations in the parameter *R* with annealing temperature. The solid line represents the exponential fit: $R = R_0 + A\ exp(b\ T)$, where $R_0 = 1.11(2)$, $A = 6.2(2) \times 10^{-5}$, and $b = 7.48(4) \times 10^{-3}$. Coefficient of determination $R^2 = 0.99$.

Figure 6c shows the variation in R as a function of temperature. The data indicate progressive recrystallization between 673 K and 1273 K in argon characterized by a single-stage mechanism. After annealing at 1273 K, the absorption line of the high-energy peak from the superposition of two Fe^{2+} components was only half the width of the corresponding line observed for the unannealed sample. The derivative of R with respect to temperature, dR/dT, is an exponential function of the inverse temperature, 1/T, and can represent the annealing rate. The derivative function shown in Figure 7a can be fitted by an Arrhenius-type equation as:

$$\left(\frac{\partial \mathbf{R}}{\partial \mathbf{T}}\right) = \mathbf{A}\mathbf{exp}\left(-\frac{\mathbf{E_A}}{\mathbf{kT}}\right) \quad (1)$$

where A = 4.592 is a fitted parameter, E_A is the activation energy, and k is the Boltzmann's constant.

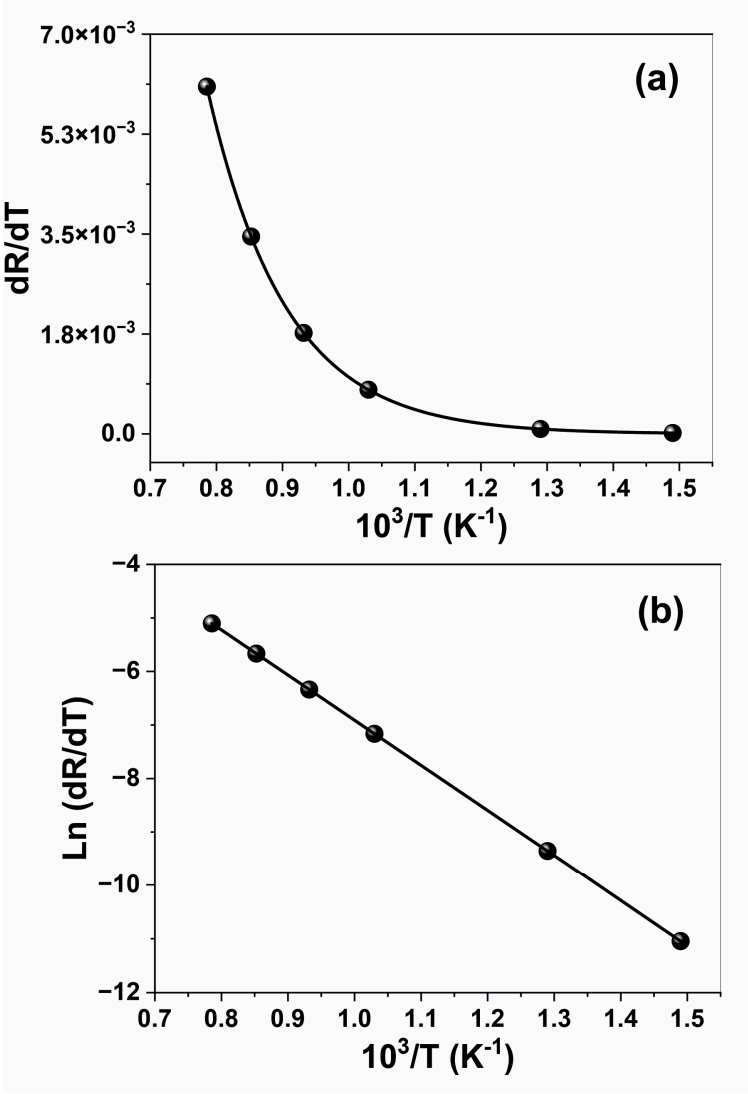

Figure 7. (**a**) Plot of $\partial R/\partial T$ vs. T^{-1}. The solid line shows the exponential fit based on Equation (1); (**b**) corresponding Arrhenius plot of $\ln(\partial R/\partial T)$ vs. T^{-1}. The solid line represents the linear regression given by Equation (2).

The logarithm of the function given by Equation (1) (Figure 7b) plotted vs. the inverse temperature is a straight line:

$$\ln\left(\frac{\partial R}{\partial T}\right) = b - \frac{1}{T}a \quad (2)$$

with slope a = 8436 and b = 1.254. Since $a = E_A/k$, the activation energy $E_A = 0.73 \pm 0.04$ eV.

The calculated activation energy of 0.73 eV for highly metamict perrierite falls well below values reported for fully metamict allanite, gadolinite, and zircon (Table 1). However, the value of 0.73 eV for metamict perrierite is comparable to the values of 0.45, 0.58, and 0.33 eV calculated for partially metamict davidite, gadolinite, and microlite [13,15,18]. In a partially metamict state, crystalline domains coexist with irregular amorphous regions. This heterogeneity can lead to lower activation energy measured during thermal recrystallization relative to that obtained from a completely metamict phase. As is the case of gadolinite, the activation energy for fully metamict perrierite is expected to be much higher. The higher activation energy estimated for perrierite relative to that reported for monazite comports with the latter's structural integrity in the presence of internal radiation and its typical natural, intact crystalline state [38,39].

4. Conclusions

^{57}Fe Mössbauer spectroscopy and XRD patterns of highly metamict perrierite annealed from 673 K to 1273 K in argon revealed progressive recrystallization with increasing annealing temperature. After annealing at 1273 K, metamict perrierite was found to be fully recrystallized and able to be indexed in the C2/m space group. The Mössbauer spectrum of the sample annealed at 1273 K consisted of two Fe^{2+} doublets representing two different structural positions and two Fe^{3+} doublets representing the same structural position but two different octahedral sites. The decrease in the width of the line of the high-energy peak from the superposition of the two Fe^{2+} components with increasing temperature may indicate the annealing rate. Based on changes in this parameter and using an Arrhenius-type equation, the activation energy for the thermal recrystallization of perrierite was determined to be 0.73 eV. Comparison of the perrierite hyperfine spectral parameters with those measured for the one sample of chevkinite analyzed thus far indicates that, within measurement uncertainty, both minerals exhibit nearly the same values for the dominant Fe^{2+} doublet, but slightly different values for the Fe^{3+} components.

Author Contributions: Conceptualization, D.M.; methodology and software, D.M., A.G. and T.K.; validation, D.M., A.G. and T.K.; investigation and measurements, D.M., M.D., A.G. and T.K., formal analysis, D.M. and T.K.; resources, D.M., M.D., T.K. and A.G.; data curation, D.M., T.K. and M.D.; writing-original draft preparation, D.M.; writing-review and editing D.M.; visualization, D.M.; funding acquisition, D.M. and M.D.; project administration, D.M. All authors have read and agreed to the published version of the manuscript.

Funding: This research was funded by the National Science Centre of Poland grant No. 2018/29/B/ST10/01495.

Data Availability Statement: The data presented in this study are available on request from the corresponding author.

Conflicts of Interest: The authors declare no conflict of interest.

References

1. Bonatti, S. Chevkinite, perrierite and epidotes. *Am. Miner.* **1959**, *44*, 115–137.
2. Jaffe, H.W.; Evans, H.T., Jr.; Chapman, R.W. Occurrence and age of chevkinite from the Devil's Slide fayalite quartz syenite near Stark, New Hampshire. *Am. Miner.* **1956**, *41*, 474–487.
3. Gottardi, G. The crystal structure of perrierite. *Am. Miner.* **1960**, *43*, 1–14.
4. Lima de Faria, J. Identification of Metamict Minerals by X-ray Powder Photographs. In *Estudos, Ensaios e Documentos*; Junta de Investigações do Ultramar: Lisbon, Portugal, 1964; Volume 112.
5. Mitchell, R.S. Virginia metamict minerals: Perrierite and chevkinite. *Am. Miner.* **1966**, *51*, 1394–1405.
6. Ito, J. A study of chevkinite and perrierite. *Am. Miner.* **1967**, *52*, 1094–1104.
7. Ito, J.; Arem, J.E. Chevkinite and perrierite: Synthesis, crystal growth and polymorphism. *Am. Miner.* **1971**, *56*, 307–319.
8. Calvo, C.; Faggiani, R. A re-investigation of the crystal structures of chevkinite and perrierite. *Am. Miner.* **1974**, *59*, 1277–1285.
9. Segalstad, T.V.; Larsen, A.O. Chevkinite and perrierite from the Oslo region, Norway. *Am. Miner.* **1978**, *63*, 499–505.
10. Parodi, G.C.; Della Ventura, G.; Mottana, A.; Raudsepp, M. Zr-rich non metamict perrierite-(Ce) from holocrystalline ejecta in the Sabatini volcanic complex (Latium, Italy). *Miner. Mag.* **1994**, *58*, 607–613. [CrossRef]
11. Sokolova, E.; Hawthorne, F.C.; Della Ventura, G.; Kartashov, P.M. Chevkinite-(Ce): Crystal structure and the effect of moderate radiation-induced damage on site-occupancy refinement. *Can. Miner.* **2004**, *42*, 1013–1025. [CrossRef]
12. Saini, H.S.; Lal, N.; Nagpaul, K.K. Annealing studies of fission tracks in allanite. *Contrib. Miner. Petrol.* **1975**, *52*, 143–145. [CrossRef]
13. Lumpkin, G.R.; Foltyn, E.M.; Ewing, R.C. Thermal recrystallization of alpha-recoil damaged minerals of the pyrochlore structure type. *J. Nucl. Mater.* **1986**, *139*, 113–120. [CrossRef]
14. Virk, S.H. Single activation energy model of radiation damage in solid state nuclear track detectors. *Radiat. Eff. Defects Solids* **1995**, *133*, 87–95. [CrossRef]
15. Janeczek, J.; Eby, R.K. Annealing in radiation damage in allanite and gadolinite. *Phys. Chem. Miner.* **1993**, *19*, 343–356. [CrossRef]
16. Meldrum, A.; Boatner, L.A.; Ewing, R.C. Displacive radiation effects in the monazite- and zircon-structure orthophosphates. *Phys. Rev. B* **1997**, *56*, 805–814. [CrossRef]
17. Malczewski, D.; Janeczek, J. Activation energy of annealed metamict gadolinite from ^{57}Fe Mössbauer spectroscopy. *Phys. Chem. Miner.* **2002**, *29*, 226–232. [CrossRef]

18. Malczewski, D.; Grabias, A.; Dziurowicz, M. Activation energy of annealed, partially metamict davidite by ^{57}Fe Mössbauer spectroscopy. *J. Geosci.* **2020**, *65*, 37–44. [CrossRef]
19. Steiger, R.H.; Jager, E. Subcommission on Geochronology: Convention on the use of decay onstants in geo- and cosmochronology. *Earth Planet. Sci. Lett.* **1977**, *36*, 359–362. [CrossRef]
20. Murakami, T.; Chakoumakos, B.C.; Ewing, R.C.; Lumpkin, G.R.; Weber, W.J. Alpha-decay event damage in zircon. *Am. Miner.* **1991**, *76*, 1510–1532.
21. Woodhead, J.A.; Rossman, G.R.; Silver, L.T. The metamictization of zircon: Radiation dose-dependent structural characteristics. *Am. Miner.* **1991**, *76*, 74–82.
22. Weber, W.J. Self-radiation damage and recovery in Pu-doped zircon. *Radiat. Eff. Defects Solids* **1991**, *115*, 341–349. [CrossRef]
23. Nasdala, L.; Wenzel, M.; Vavra, G.; Irmer, G.; Wenzel, T.; Kober, B. Metamictisation of natural zircon: Accumulation versus thermal annealing of radioactivity-induced damage. *Contrib. Miner. Petrol.* **2001**, *141*, 125–144. [CrossRef]
24. Malczewski, D.; Dziurowicz, M. ^{222}Rn and ^{220}Rn emanations as a function of the absorbed α-doses from select metamict minerals. *Am. Miner.* **2015**, *100*, 1378–1385. [CrossRef]
25. Malczewski, D.; Dziurowicz, M.; Krzykawski, T.; Grabias, A. Spectroscopic characterization and thermal recrystallization study of an unknown metamict phrase from Tuften Quarry, southern Norway. *Can. Miner.* **2018**, *56*, 365–373. [CrossRef]
26. Dollase, W.A. Mössbauer spectra and iron distribution in the epidote-group minerals. *Z. Krist. Cryst. Mater.* **1973**, *138*, 41–63.
27. Ito, J.; Hafner, S.S. Synthesis and study of gadolinites. *Am. Miner.* **1974**, *59*, 700–708.
28. Kartashov, P.M.; Ferraris, G.; Ivaldi, G.; Sokolova, E.; McCammon, C.A. Ferriallanite-(Ce), $CaCeFe^{3+}AlFe^{2+}(SiO_4)(Si_2O_7)O(OH)$, a new member of the epidote group: Description, X-Ray and Mössbauer study. *Can. Miner.* **2002**, *40*, 1641–1848. [CrossRef]
29. Malczewski, D. Recrystallization in fully metamict gadolinite from Ytterby (Sweden), annealed in air and studied by ^{57}Fe Mössbauer Spectroscopy. *Am. Miner.* **2010**, *95*, 463–471. [CrossRef]
30. Hawthorne, F.C.; Groat, L.A.; Rausepp, M.; Ball, N.A.; Kimata, M.; Spike, F.D.; Gaba, R.; Halden, M.N.; Lumokin, G.R.; Ewing, R.C.; et al. Alpha-decay damage in titanite. *Am. Miner.* **1991**, *76*, 370–396.
31. Malczewski, D.; Grabias, A. ^{57}Fe Mössbauer Spectroscopy of radiation damaged allanites. *Acta Phys. Pol. A* **2008**, *114*, 1683–1690. [CrossRef]
32. Reissner, C.E.; Bismayer, U.; Kern, D.; Reissner, M.; Park, S.; Zhang, J.; Ewing, R.C.; Shelyug, A.; Navrotsky, A.; Paulmann, C.; et al. Mechanical and structural properties of radiation-damaged allanite-(Ce) and the effects of thermal annealing. *Phys. Chem. Miner.* **2019**, *46*, 921–933. [CrossRef]
33. Li, Z.; Jin, M.; Liu, M.; Liu, X. Iron distribution in chevkinite. *Hyperfine Interact.* **1992**, *70*, 1057–1060. [CrossRef]
34. Hawthorne, F.C. (Ed.) Spectroscopic methods in mineralogy and geology. Reviews in mineralogy. *Miner. Soc. Am.* **1988**, *18*, 698.
35. Rancourt, D.G.; Dang, M.Z.; Lalonde, A.E. Mössbauer Spectroscopy of tetrahedral Fe^{3+} in trioctahedral micas. *Am. Miner.* **1992**, *77*, 34–43.
36. Primak, W. Kinetics of processes distributed in activation energy. *Phys. Rev.* **1955**, *100*, 1677–1689. [CrossRef]
37. Primak, W. Large temperature range annealing. *J. Appl. Phys.* **1960**, *31*, 1524–1533. [CrossRef]
38. Ewing, R.C.; Haaker, R.F. The metamict state: Implications for radiation damage in crystalline waste forms. *Nucl. Chem. Waste Manag.* **1980**, *1*, 51–57. [CrossRef]
39. Meldrum, A.; Boatner, L.A.; Weber, W.J.; Ewing, R.C. Radiation damage in zircon and monazite. *Geochim. Cosmochim. Acta.* **1998**, *62*, 2509–2520. [CrossRef]